ISSN 1070-3632, Russian Journal of General Chemistry, 2010, Vol. 80, No. 6, pp. 1152–1167. © Pleiades Publishing, Ltd., 2010.
Original Russian Text © R.A. Evarestov, A.B. Bandura, M.V. Losev, 2010, published in Zhurnal Obshchei Khimii, 2010, Vol. 80, No. 6, pp. 982–998.

# Symmetry and Stability of Nanotubes Based on Titanium Dioxide

**R. A. Evarestov, A. B. Bandura, and M. V. Losev**

*St. Petersburg State University, Universitetskii pr. 26, St. Petersburg, 198504 Russia*
*e-mail: re1973@re1973.spb.edu*

Received January 21, 2010

**Abstract**—The process of rolling a monolayer of bulk crystal with biperiodical planar lattice to the nanotube was analyzed. It was shown by an example of the carbon nanotubes how the tube symmetry can be revealed through the analysis of symmetry of graphene layers (the layer group with a hexagonal planar lattice) and its changes at the rolling to form the tube. The developed approach can be used to analyze the symmetry of any nanotube. A computer program we developed is discussed that allows to determine the nanotube symmetry using the data on the symmetry and coordinates of the atoms in the nanolayer and get the coordinates of the atoms in the unit cell of the nanotube which can be used for the further quantum-chemical calculations. The method and results of ab initio calculations of the titanium dioxide monolayer stability in the LCAO basis optimized for the bulk crystal, using the hybrid exchange-correlation potential PBE0 are presented. Symmetry properties of nanotubes obtained by rolling the three- and six-plane monolayers (101) and (001) of anatase are discussed. Atomic and electronic structure of $TiO_2$ nanotubes found by geometry optimization is analyzed. It is shown that titanium dioxide nanotubes based on the three-plane monolayers with hexagonal and square lattice are approximately of the same stability. The data on the stability of nanotubes are essential for the synthesis of new nanomaterials based on titanium dioxide.

**DOI:** 10.1134/S1070363210060198

Discovery of fullerenes in 1985 and carbon nanotubes in 1991 was a principal point in the development of a new field of science, the chemistry and physics of nanostructures. Soon afterwards, in 1995, the nanotubes of more complex structure based on the metal oxides have been synthesized. To date, a considerable amount of information about these nanotubes was accumulated, the methods for their synthesis have been developed, the ways of modification of their properties and creation of new oxide nanostructures were defined [1]. It is fair to say that a new field of inorganic chemistry has born–the chemistry of nanostructures.

Although the first oxide-based nanotubes (often called inorganic) were obtained almost simultaneously with the discovery of carbon nanotubes, the majority of scientific papers on inorganic nanotubes is still devoted to new methods for their synthesis. Physical and chemical properties of inorganic nanotubes were studied much less than the properties of carbon nanotubes. No doubt that the properties of nanomaterials differ from the properties of related stable crystalline phases. Therefore, theoretical simulation of the nanotubes stability, chemical and physical properties, currently plays a key role and stimulates further, more detailed study of known nanomaterials pointing to the synthesis of new ones.

The development of computer technology in the last 10–20 years provided rapid progress of computational methods in quantum chemistry. Thank to this, nonempirical calculations of molecules and crystals become quite a routine procedure. However, simulation of nanosystems is a new challenge in the field of computer simulation. Sizes of these objects are by orders of magnitude larger than the size of conventional molecular systems: even the simplest carbon nanotubes contain thousands or even tens of thousands of atoms [2]. At the same time, nanoparticles do not have a three-dimensional periodicity, such as three-dimensional crystals widely considered as the objects of computer simulation. Translational symmetry of a crystal allows the restriction of the calculation to account explicitly only for the atoms of one unit cell that provides the possibility of the quantum-chemical calculations of crystals. There is no doubt that only the development of supercomputer technology can provide a quantum-mechanical simulation of nanosystems, and as a consequence, to

lead to the creation of the necessary theoretical framework for the development of nanotechnology.

However, the nanotubes are an example of the nanosystems whose properties can now be studied by the modern ab initio methods of quantum chemistry. Indeed, the nanotubes have an advantage over other nanoobjects: like polymers, they have a periodicity in one dimension. This allows, as in the case of crystals, to reduce the calculation to one unit cell. However, for nanotubes with realistic diameters, a cylindrical unit cell will contain hundreds or even thousands of atoms. Here another remarkable property of nanotubes can assist, their axial symmetry. Many of the nanotubes have simple or screw axis of high order. A turn around the axis, and in the case of screw axis a simultaneous translation along the tube axis transfers a tube into itself. These symmetry elements make nanotubes more promising objects for the quantum-chemical simulation than, for example, nanoclusters, the compact nanoparticles with the point symmetry characteristic for molecules.

Among the numerous inorganic nanotubes obtained to date, the nanotubes based on titanium dioxide ($TiO_2$) are of most practical interest because of the huge potential of their applications. Owing to their high photocatalytic activity, strong oxidizing ability and, at the same time, chemical inertness, as well as unique optical properties, the nanomaterials based on the titanium dioxide are able to revolutionize the creation of various electro-optical and electro-chemical systems that can be used as efficient power sources, gas sensors operating at high temperatures, devices for the decomposition of water using solar energy, nanofilters for air purification and carbon dioxide consumption.

Titanium dioxide exists in three different crystalline modifications: anatase, rutile and brookite. Experiments on electron diffraction indicate that the nanotubes are formed on the basis of the structure of anatase, possibly with some admixture of rutile.

For the synthesis of nanotubes a method of precipitation from solutions of titanium salts is used. Depending on the synthesis procedure, the diameter of a nanotube can vary from tenths to tens of nanometers. Initially two-dimensional lamellar structures are formed, which then spontaneously roll up into a tube. Thus it seems that the nature gives a hint: first should be examined a nano-sheet, the monolayer or a sheet formed by one or more atomic layers, and then can be explored a possibility of its rolling up into the nanotube, with simultaneous analysis of the changes in symmetry, atomic structure, and energy at this transformation. This approach is implemented in this work.

Section 1 contains the discussion of the procedures for the rolling a monolayer of bulk crystal with biperiodical flat lattice into a nanotube. By an example of carbon nanotubes we show how to reveal the tube symmetry through analysis of symmetry of graphene layers (layer group with a hexagonal planar lattice) and its changes at rolling up to the tube. The developed approach can be used to analyze symmetry of any nanotube. In section 2 we briefly consider a computer program we developed that allows to determine the symmetry of nanotube using the data on symmetry and coordinates of the atoms in the nanolayer and to obtain the coordinates of the atoms in the unit cell of the nanotube to use them for further quantum-chemical calculations. In Section 3 we discuss the method of calculation of oxide monolayers in the LCAO basis optimized for the bulk crystal, using hybrid exchange-correlation potential PBE0. Section 4 treats the symmetry and stability of different monolayers of titanium oxides $TiO_2$ and the models of nanotubes based on them. In Section 5 we analyze the calculated atomic and electronic structures of nanotubes obtained by rolling up the anatase (101) and (001) monolayers with geometry optimization. Finally we conclude on the stability of titanium dioxide nanotubes in various models.

## 1. Symmetry Relations Between the Nanolayers and Nanotubes

Analysis of symmetry of nanotubes is based on the consideration of procedures for the rolling up nanolayers. As an example, let us consider a monolayer of graphite (graphene), see Fig. 1. This monolayer contains two carbon atoms in a unit cell of hexagonal lattice with primitive translation vectors **a** and **b** at an angle of 60° and having the same length $a = d \cdot 3^{1/2} = 2.46$ Å (the bond length between adjacent carbon atoms in graphite $d = 1.42$ Å). Rolling the graphene layer to obtain a single-wall nanotube means placing the carbon atoms on the surface of a cylinder. The number of atoms is determined by the rolling vector (called chirality vector) $\mathbf{R} = n_1\mathbf{a} + n_2\mathbf{b}$, whose length $R = \pi D$ determines the tube diameter $D$. The integers $n_1$ and $n_2$ define the so-called nanotube chirality.

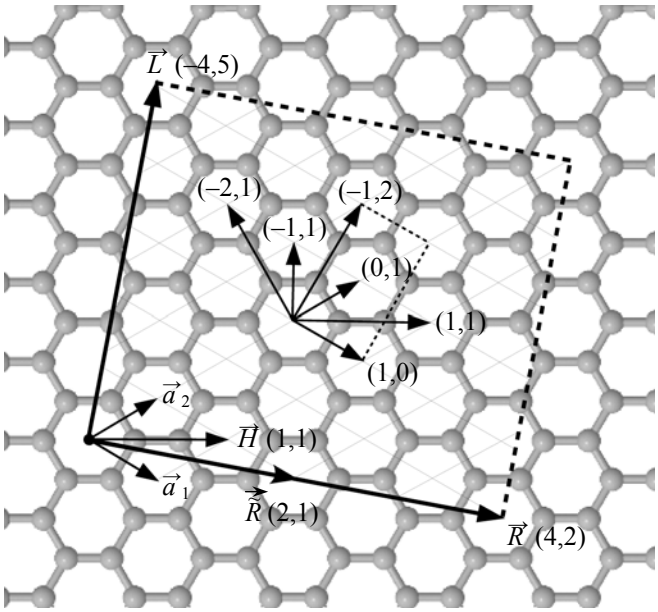


**Fig. 1.** Chirality vectors of the nanotubes from graphene layer.

Translational symmetry of monoperiodical nanotube is determined by the translation vector **L** = $l_1$**a** + $l_2$**b** along the tube axis, which is orthogonal to the chirality vector. From the orthogonality condition (**RL**) = 0 the ratio between integers $l_1$ and $l_2$ can be found which for a planar obliquelattice (the primitive translation vectors are of different length, the angle between them $\gamma \neq 90°$) has the form (1).

$$\frac{l_1}{l_2} = -\frac{n_2a^2 + n_1ab\cos\gamma}{n_1b^2 + n_2ab\cos\gamma}. \qquad (1)$$

For the hexagonal lattice $a = b$, $\gamma = 60°$, and the ratio (1) takes the form (2).

$$\frac{l_1}{l_2} = -\frac{2n_2 + n_1}{2n_1 + n_2}. \qquad (2)$$

The chirality vector **R** may consist of a number (integer) of the vectors of smaller length, $\tilde{\mathbf{R}}$ = **R**/$n$ = $\tilde{n}_1$**a** + $\tilde{n}_2$**b,** where $\tilde{n}_1 = n_1/n$, $\tilde{n}_2 = n_2/n$. Vector $\tilde{\mathbf{R}}$ is called the reduced chirality vector. The relation (2) implies that all the tubes with chirality vectors **R** = $n\tilde{\mathbf{R}}$ ($n$ = 1, 2, 3, ...) have the same period. Fig. 1 shows the chirality vector **R**(4,2) = 2$\tilde{\mathbf{R}}$ (2,1). The reduced chirality vector $\tilde{\mathbf{R}}$ (2,1) is the same for all tubes of type (2$n$,$n$), the translational symmetry is determined by the same vector **L**(–4,5). There are three types of graphene tubes: ($n$,0) of *zigzag* type, ($n$,$n$) of *armchair* type, and ($n_1$, $n_2$) corresponds to the tubes of general type. In particular, $l_1/l_2$ = –1/2 and –1 for the graphene tubes of ($n$,0) and ($n$,$n$) types, respectively. The tubes (2$n$,$n$) are of general type, for which $l_1/l_2$ = –4/5.

Figure 2 shows the extended unit cells (EUC) of hexagonal lattice constructed on the vectors **R** and **L**. By rolling them along the chirality vectors **R**(3,0), **R**(3,3) and **R**(6,3) the tubes are formed of the types *zigzag, armchair,* and of general type, respectively. Each of these three chirality vectors consists of three ($n$ = 3) vectors of smaller length, $\tilde{\mathbf{R}}$(1,0), $\tilde{\mathbf{R}}$(1,1), and $\tilde{\mathbf{R}}$(2,1), respectively. Also the corresponding translation vectors are shown of the tubes derived from the relation (2). The number of carbon atoms in the graphene tubes is determined by the doubled number of the nodes in the corresponding EUC, that, is, by the doubled determinant $q$ of the matrix

$$\mathbf{Q} = \begin{pmatrix} n_1 & n_2 \\ l_1 & l_2 \end{pmatrix}$$

of transition from the primitive translation vectors **a** and **b** to the translation vector **R** and **L** of the EUC for the corresponding tube. In particular, for the tubes shown in Fig. 3, $q$ = 6, 6 and 42, and the number of atoms in EUC is 12, 12 and 84, respectively. Obviously, the determinant $\tilde{q} = q/n$ of the matrix

$$\tilde{\mathbf{Q}} = \begin{pmatrix} \tilde{n}_1 & \tilde{n}_2 \\ l_1 & l_2 \end{pmatrix}$$

determines the minimum possible number of the nodes in the EUC for a tube of a given type [in our example $\tilde{q}$ = 2, 2, and 14 for the tubes (1,0) (1,1) and (2,1), respectively]. For the tubes of this type, increase in $n$ means only an increase in the tube diameter, while its translation vector and symmetry remain the same.

We now turn to the analysis of the symmetry of graphene nanotubes. This analysis proceeds from the layer symmetry group (biperiodical) of the layer to be rolled and is based on the revealing the symmetry operations of the layer groups which "survive" at the rolling up the layer into the tube.

The symmetry group of graphene layer $P6/mmm$ (number 80 in the list of 80 layer groups [3]) contains all translations of hexagonal lattice and the following operations of the point group symmetry $D_{6h}$: six rotations around the main axis of sixth order perpendicular to the plane of the layer (let this axis to coincide with the $z$ axis), reflection in the lattice plane perpendicular to this axis, and reflections in the planes

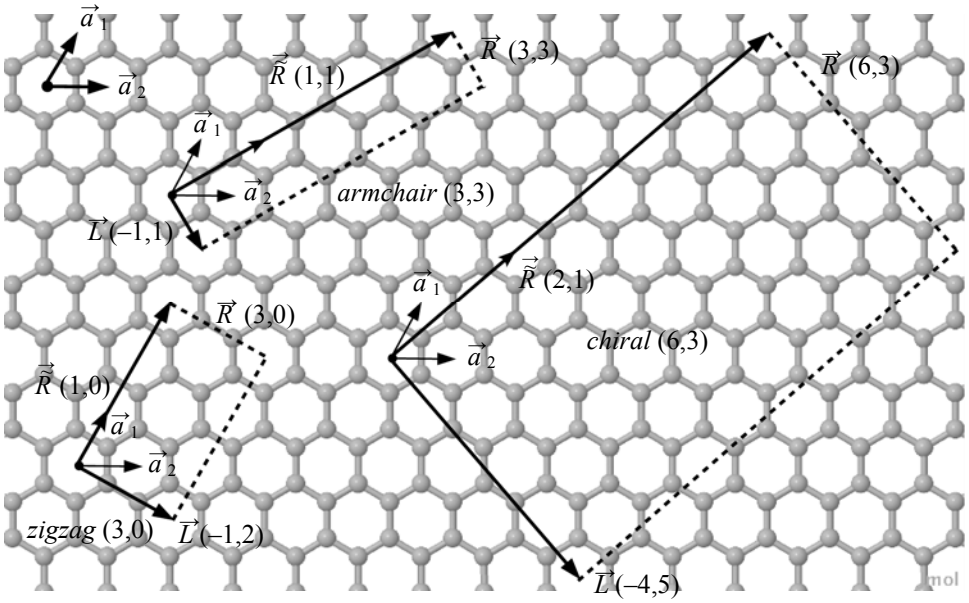


**Fig. 2.** Extended unit cells of graphene layer.

passing through the main axis. These planes form two groups, three planes in each. The planes of the first group pass through the vertices of a hexagon, and are defined by the translation vector (1,1), (–1,2), and (–2,1), see Fig. 1. The planes of the second group pass through the middle of the hexagon sides, and are defined by the translation vector (1,0) (0,1), and (–1,1), see Fig. 1.

At the rolling up the graphene layer into the tube, of 6 rotations around the principal axis remains only a 180° rotation maintaining the translational symmetry along the tube axis. Reflection in the plane perpendicular to the principal axis is no longer a symmetry element, because the plane of layer becomes the surface of the cylinder. Reflections in planes perpendicular to the plane of the layer become for the tube the reflections $\sigma_h$ and $\sigma_v$ in planes perpendicular or parallel to its axis (to translation vector **L**). At choosing the chirality vector **R** along any of the vectors defining the reflection planes of the first group, the tube translation vector **L** will be directed along the vector translation of the hexagonal lattice orthogonal to it that defines a plane of the second family. As seen from Fig. 1, when the vector (1,1) is taken as a chirality vector, the orthogonal to it translation vector (–1,1) becomes a translation vector of the tube. Therefore, the symmetry plane of the layer defined by the vector (1,1) will become the tube symmetry plane $\sigma_h$ perpendicular to the tube axis. Obviously, for the considered pair of the vectors of layer translation the chirality and the tube translation vectors can be interchanged. In this case, the symmetry plane of the layer defined by the vector (1,1) becomes for the tube the symmetry plane $\sigma_v$ parallel to the tube axis.

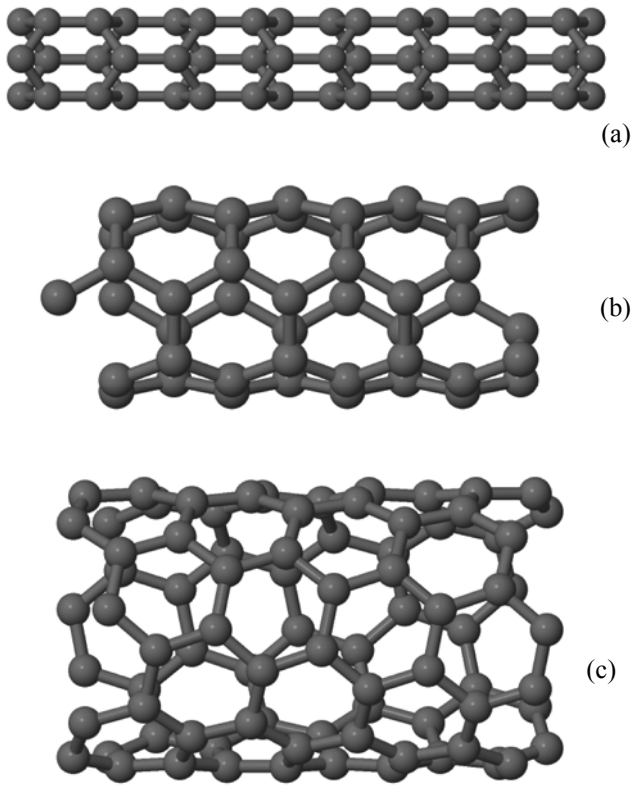


**Fig. 3.** Graphene nanotubes: (a) *zigzag*, (b) *armchair*, and (c) *chiral* (6,3).

Thus, at rolling up the graphene layer into the tube, among the symmetry planes perpendicular to the tube axis or passing through it retain only those connected with the chirality vectors associated with the symmetry planes perpendicular to the plane of the rolled layer. At the same time, the rotation around the tube axis by 180° will be a symmetry operation for graphene tubes of any chirality. From the foregoing it is clear that the mutually equivalent *zigzag* tubes correspond to the chirality vectors $(n,0)$, $(0,n)$ and $(n,n)$, and mutually equivalent *armchair* tubes correspond to the chirality vectors $(n,n)$, $(-n,2n)$, and $(-2n,n)$. Therewith the symmetry operation will be reflection in the plane perpendicular to the tube axis. For all common types of tubes with chirality vectors $(2n,n)$ among the symmetry operations of graphene layers "survive" only the rotations 180° around the axis perpendicular to the layer plane.

We now consider the tube symmetry operations arising from the translation of graphene layer. Upon rolling to the tube, each of $q = n\tilde{q}$ translations from the corresponding EUC becomes a turn around the axis of the tube, a simple $C_n$ by an angle $2\pi/n$ (where $n > 1$), or screw turn $T_q^r = (C_q^r \mid 1/\tilde{q})$ by an angle $2\pi r/q$ ($r$ is an integer value) with simultaneous translation by $\mathbf{L}/\tilde{q}$ (at $\tilde{q} > 1$). As seen from Fig. 1, for any choice of the chirality vectors of a graphene tube (such as *zigzag* or *armchair*) the minimal EUC built on the vectors **R** and **L** contains two nodes of the original hexagonal lattice ($\tilde{q} = 2$), so that a rotation by the angle $2\pi/q$ will be accompanied by a translation equal to a half vector of the tube translation.

Summarizing all the above, we conclude that the graphene tubes of any chirality belong to the point group $D_q$, and for a specific choice of chirality vectors $\mathbf{g} \in \{(n,0), (0,n), (-n,n)\}$ or $\mathbf{h} \in \{(n,n), (-n,2n), (-2n,n)\}$ the tube point symmetry increases to $D_{2nh}$. Here we use the symbols **g** and **h** for the two nonequivalent sets of chirality according to [4].

The symmetry operation of the nanotube can be characterized by the vector of screw turns $\mathbf{H} = h_1\mathbf{a} + h_2\mathbf{b} = (r/n\tilde{q})\mathbf{R} + (1/\tilde{q})\mathbf{L}$, whose components describe the rotational and translational part of the screw rotation $T_q^r$. The cell built on the translation vectors $\tilde{\mathbf{R}}$ and **H** is equal to the area of the primitive cell under the conditions $\tilde{n}_1 h_2 - \tilde{n}_2 h_1 = 1$, which is used to find the components of the vector **H**. The rotational component of the vector **H** is determined by the value $r = h_1 l_2 - h_2 l_1$, and its translational component, by $\tilde{q} = q/n$. Figures 1 and 2 show the vector **H** for each chirality vector. Thus, for the tubes of the type $(2n,n)$, $h_1 = h_2 = 1$, $q = 14n$, $r = 9$, and $\tilde{q} = 14$ (Fig. 1).

For each of the 80 layer groups the symmetry of the nanotubes can be considered obtained on the basis of the group, just as was done for the layer group of ghraphene symmetry. For the tubes with the general type chirality, when in the layer group there is no symmetry axes of order 2, 4, or 6, perpendicular to the plane of the layer, this gives a monoperiodical group with the point symmetry $C_q$, otherwise, in the presence of such axis the tube point symmetry increases to $D_q$. For each of the four plane lattices (hexagonal, square, rectangular centered and simple) one can specify a particular choice of chirality that increases the symmetry of the tube to one of the five point group: $S_{2n}$, $C_{nv}$, $C_{nh}$, $D_{nd}$, and $D_{nh}$. These groups (along with the groups $C_n$ and $D_n$) are called the groups of axial symmetry, as the corresponding operations retain the axial symmetry of the object, and at the presence of periodicity along the axis retain translational symmetry. Monoperiodical symmetry group (in the English literature they are called LINE groups) have been known for a long time for so-called stereoregular polymers [5], while for the nanotubes they are used relatively recently [6]. Total number of the monoperiodical groups equals to infinity, but they are divided into 13 families [4]. In particular, the symmetry group of the graphene tubes belong to the family 13 (for *zigzag* and *armchair* tubes) and to the family 5 (for all other tubes), with point symmetry $D_{nh}$ and $D_n$, respectively. The family 1 includes all monoperiodical groups with point symmetry $C_n$. The so-called ROD groups [3] form a finite subset in the infinite number of the monoperiodical groups. The ROD groups have been introduced in crystallography and are subgroups of space group symmetry of bulk crystals (the symmetry axis in such groups may be of the order 2, 3, 4, and 6).

Note that the symmetry of a nanotube rolled from a nanolayer is determined not only by the type of the respective planar lattice, but also by the operations which form a layer group (a layer group may comprise a part of the symmetry operations of the planar lattice). In addition, if two surfaces of a nanolayer are not equivalent (that is, there are no operations that transform one surface to another), at the rolling up the nanotubes of two types of the same symmetry are formed but differing by the structure of the inner and outer surfaces.

Table 1 compiled from [4] shows the distribution over the families of symmetry groups of the nanotubes obtained by rolling up the layers of different symmetry. Groups of the first family $L^{(1)}$ describe the symmetry of the tubes for the layer groups without second-order rotation axis perpendicular to the plane of the layer, the family group 5 relates to the layer groups with such axis. Numbering of the layer groups is given in accordance with the International Tables [3]. Underlining the number of a layer group means that at the rolling up the layer to the tube the symmetry of the latter may rise for some chirality vector, collectively designated by Latin letters **a**, **b**, **c**, . . In the families 2, 3, 6, 9, and 11 the monoperiodical groups are symmorphic, that is, they do not include rotations around the screw axes and reflections in the glide planes. For some groups with a hexagonal and square or centered rectangular lattice a doubling of the rotation axis of the order $n$ occurs ($n$ is defined by the choice of the chirality vector): the families 4, 8, and 13. Finally, the groups of families 7, 10, and 12 include a reflection in the plane passing through the tube axis, with a translation by a half the translation vector along the tube axis.

Using the information in the Table 1, we propose the following method of determining the symmetry of a nanotube obtained by rolling up the layer cut from a bulk crystal. In the bulk crystal is cut a layer, whose symmetry is described by one of the 80 layer groups. From Table 1 the possible families are determined, which may include the symmetry group of the nanotube with a particular choice of the chirality vector. For each such choice the components of the translation vector **L** are computed and of the vector of screw rotation **H** and thus a complete set of symmetry operations of the nanotube is determined. The number of atoms in the nanotube cell is determined by the product of the number of translations $q$ and the number of atoms in the primitive cell of the layer. Symmetry group of a nanotube may contain a sufficiently large number of symmetry operations, which increases with the diameter of the nanotube. Thus, the graphene tube

**Table 1.** Correspondence between biperiodical (layer) and monoperiodical groups of the nanotubes obtained by the rolling up monolayers [4]

| Family | Monoperiodical group | | Point group | Biperiodical groups[b] |
|---|---|---|---|---|
| | even $n$ | odd $n$ | | |
| 1[a] | $\mathbf{L}q_p$ | | $C_q$ | 1,2,4,5,8,9,10,11,12,13,14,15,16,17,18,27,28,29,30,31,32,33,34,35,36,65, 66,67,68,69,70,71,72,74,78,79 |
| 5[a] | $\mathbf{L}q_p22$ | $\mathbf{L}q_p2$ | $D_q$ | 3,6,7,19,20,21,22,23,24,25,26,37,38,39,40,41,42,43,44,45,46,47,48,49,50, 51,52,53,54,55,56,57,58,59,60,61,62,63,64,73,75,76,77,80 |
| 2 | $\mathbf{L}(2n)$ | $\mathbf{L}\bar{n}$ | $S_{2n}$ | *a*: 17,33,34; *b*: 12,16,29,30 |
| 3 | $\mathbf{L}n/m$ | $\mathbf{L}(2n)$ | $C_{nh}$ | *a*: 11,14,15,27,31,32; *b*: 28 |
| 4 | $\mathbf{L}(2n)_n/m$ | | $C_{2nh}$ | *e*: 13,18,35; *d*: 36; *h*: 69,72,78; *g*: 70,71,79 |
| 6 | $\mathbf{L}nmm$ | $\mathbf{L}nm$ | $C_{nv}$ | *a*: 28; *b*: 11,14,15,27,31,32 |
| 7 | $\mathbf{L}ncc$ | $\mathbf{L}nc$ | $C_{nv}$ | *a*: 12,16,29,30; *b*: 17,33,34 |
| 8 | $\mathbf{L}(2n)_nmc$ | | $C_{2nv}$ | *e*: 36; *d*: 13,18,35; *h*: 70,71,79; *g*: 69,72,78 |
| 9 | $\mathbf{L}(2n)2m$ | $\mathbf{L}\bar{n}m$ | $D_{nd}$ | *a*: 42,45; *b*: 24,38,40 |
| 10 | $\mathbf{L}(2n)2c$ | $\mathbf{L}\bar{n}c$ | $D_{nd}$ | *c*: 25,39,43,44,56,60,62,63 |
| 11 | $\mathbf{L}n/mmm$ | $\mathbf{L}(2n)2m$ | $D_{nh}$ | *c*: 23,37,41,46,55,59,61,64 |
| 12 | $\mathbf{L}n/mcc$ | $\mathbf{L}(2n)2c$ | $D_{nh}$ | *a*: 24,38,40; *b*: 42,45 |
| 13 | $\mathbf{L}(\bar{2}\bar{n})_n/mcm$ | | $D_{2nh}$ | *f*: 26,47,48,55,56,57,58,61,62,63,64; *i*: 77,80 |

[a] In the international notation of screw axes $p = n$ ($r^{-1} \bmod \tilde{q}$) (see text). In families 1 and 5 are emphasized the biperiodical groups which at the rolling with the use of special chirality vectors fall to the other families of monoperiodical groups. [b] Special chirality vectors: $a = (n, 0)$, $b = (0,n)$, $c \in \{(n, 0), (0, n)\}$, $d = (n, n)$, $e = (-n,n)$, $f \in \{(n, n), (-n, n)\}$, $g \in \{(n, 0), (0, n), (-n, n)\}$, $h \in \{(n, n), (-n, 2n), (-2n, n)\}$, $i \in \{(n, 0), (0, n), (-n, n), (n, n), (-n, 2n), (-2n, n)\}$. Distribution of rectangular biperiodical groups over the special chirality vectors, generally speaking, depends on the settings at selecting the main axes.

with the chirality ($n$,0) and ($n$,$n$) contains 4$n$ atoms and 8$n$ symmetry operations, whose rotating parts form the group $D_{2nh}$.

In this paper the determination of the symmetry of specific nanotubes and of the atomic coordinates in the nanotubes was carried out on the basis of a computer program that we have developed, briefly described in the next section.

## 2. Computer Program for Determining the Symmetry of the Nanotubes and the Building of Atomic Coordinates

To determine the symmetry of specific nanotubes and to reveal atomic coordinates of the nanotube, we have developed a computer program "NTsym." The program is written in high level programming language Python [7], applying the principles of object-oriented programming. At developing the program we used third-party libraries, and, in particular, a library for manipulating with a set of atoms ASE [8]. To find the space group, in the program both spglib library [9], and the program FINDSYM, the part of a complex ISOTROPY were used [10]. Details of the algorithm are described below.

Program "NTsym" focuses on the use of a software package CRYSTAL06(09) [11]. It processes the output files of this package to extract the geometry of nanolayer of a bulk crystal, both before and after relaxation of its structure. Construction of a nanolayer is carried out using CRYSTAL06(09) by cutting out a given number of atomic planes from the bulk crystal. The resulting structure of the nanolayer can be reconstructed and then is used as input in the program "NTsym" to determine the sectors of the layer group.

The number of atomic planes is determined unambiguously by the $z$-coordinate of the atoms of the nanolayer, and for determining the layer group the following algorithm is used. For a biperiodical nanolayer (with two translation vectors in the layer plane) the third translation vector of arbitrary length is constructed, orthogonal to the first two translation vectors. The result is a triperiodical structure which is equivalent to the model of periodic slab (this model is used in the calculations of the crystal surface in the basis of the planar waves). The symmetry of the obtained triperiodical structure is characterized by a space group. To determine the space group of an arbitrary triperiodical structure from the lattice parameters and coordinates of all atoms in the unit cell FINDSYM program is used, its algorithm has been described in [10]. Since the layer group is a sub-periodical subgroup of space group, then after determining the space group it is easy to find relevant layer group using the International Tables for Crystallography, Volume E [3]. After finding the layer group of the nanolayer, Table 1 is used in the NTsym program for the determination of the possible chirality vectors both of general type and those which would increase the nanotube symmetry. For a given chirality vector **R** defined by the vectors of primitive cell of the layer the program "NTsym" computes the translation vector **L** orthogonal to the chirality vector and the vector **H**. Next, an extended unit cell (EUC) is constructed on the vectors **R** and **L**, which contains $q$ primitive cells of the layer. The obtained EUC is rolled along the vector **R** to obtain the coordinates of the atoms in the nanotube defined by the indices of the chirality vector. Therewith the method is used developed in [12]. Finally, from Table 1 the information is extracted about the complete symmetry of the nanotube. Output file containing the coordinates of atoms of the nanotube is used for computing with the program CRYSTAL06(09) [11].

The program we developed can be used for the calculations of multiwall nanotubes obtained by rolling of two or more nanolayers when for each layer is selected its own chirality vector. Here we restrict ourselves by considering two-wall nanotubes. Two cases are possible.

In the first case the ratio $l_1/l_1$ for the two nested nanotubes is the same. Both the tubes are called commensurable. They have the same translation vector, which becomes the translation vector for the obtained two-wall nanotube. This is the case, for example, of discussed in [13] two-wall carbon nanotubes of the type $n(\tilde{n}_1,\tilde{n}_2)@m(\tilde{n}_1,\tilde{n}_2)$ (in this notation, the symbols left of the @ indicate chirality of the inner tube and right that of outer one).

In the second case (incommensurate nanotubes) our program searches for a translation vector common for the two tubes, which is determined approximately with some accuracy. The ratio of the vectors of translation is approximated with the required accuracy by a rational fraction $n/m$ so that the translation vector of the two-wall tube is defined as $na_{in} \approx ma_{out}$ ($a_{in}$ and $a_{out}$ denote the length of the translation vectors of inner and outer nanotubes, respectively).

To calculate the electronic structure of $TiO_2$ nanotubes, in the present study the program

CRYSTAL06(09) is used in which the symmetry is realized only for the ROD group. Therefore, for nanotubes with $q \neq 2, 3, 4, 6$ all calculations were performed with a partial accounting for the symmetry. However, for some double-walled nanotubes, the total symmetry is sufficiently low [13], so that it can be accounted for without going beyond the use of ROD groups.

### 3. The LCAO-PBE0 Calculation Scheme

For the calculation of the nanolayers and nanotubes we used LCAO method and hybrid exchange-correlation potential PBE0 [14]. This option of the calculation scheme is defined by the following. Unlike the basis of plane waves (PW), the use of atomic basis is not connected with the need to introduce an artificial three-dimensional periodicity and therefore the structures with a low periodicity, the biperiodical nanolayers and monoperiodical carbon nanotubes can also be considered. At the same time, the calculations in the PW basis are always associated with the need to achieve convergence of the results at the increase in the period of the nanolayer or nanotube. Note that the method of cylindrical augmented planar waves [15] focuses on the monoperiodical systems and therefore allows the calculation of the electronic structure of nanotubes without artificial introduction of three-dimensional periodicity and with complete accounting for the symmetry. Practical implementation of this method to date was carried out only for the nanotubes on the basis of graphite and hexagonal boron nitride.

While selecting the exchange-correlation potential we considered a necessity of reliable reproducing the gap of forbidden band that is an important characteristic of inorganic nanostructures. It is known that the Hartree-Fock or density functional calculations lead to noticeable error in the band gap (overestimation or underestimation, respectively). However, in calculations with hybrid exchange-correlation potential the gap for bulk crystals is reproduced quite well [16].

For the titanium atom we used the "small core" pseudopotential [17] (3*s*, 3*p*, 3*d* and 4*s* electrons are considered as valence) and the related non-contracted Gaussian type basis. For the oxygen atom we used full-electron Gaussian basis 6-311(d) [18]. It is known that at the calculating a crystal, the basis for a free atom should be modified by the deleting or varying diffuse atomic functions [16]. In this work, from the atomic basis we excluded the Gaussian functions with exponents less than 0.1, so the atomic basis for titanium included 5 functions of the *s*-type, 6 of *p*-type, and 5 of *d*-type. Therewith, we optimized the exponents of 4 most diffuse Gaussian functions of titanium: one for each *s*- and *p*-function and two for the functions of *d*-type), and for oxygen atom were optimized exponents of three Gaussian functions (two of *sp*-type and one of *d*-type).

To optimize the basis we used the Powell's method of "conjugate directions" [19] as one of the most effective methods for optimizing functions of several variables. In the software complex OPTBAS developed by us [20] the optimization of exponents by the Powell's method is performed through the computation of energy with the use of the computer code CRYSTAL06(09) included in the software package. This allows the optimization of the basis for the bulk crystal, nanolayers and nanotubes.

Summation over the Brillouin zone was carried out along the Monkhorst-Pack scheme [21]: the sets 888, 881 and 811 were used for three-dimensional crystals, nanolayers and nanotubes, respectively. The self-consistence procedure was carried out with an accuracy of $10^{-6}$ eV of the total energy per a cell. The need in the high precision in the calculations is defined by the necessity to calculate the small difference of large quantities of energy at the estimation of the energy of formation of nanolayers and nanotubes.

The developed scheme provides sufficiently high reliability of the obtained results as demonstrates the fact that we found both structural (tetragonal lattice constants *a*, *c,* and the parameter *u* defining the position of the oxygen atom in the cell) and electronic (atomization energy $E_{coh}$, forbidden band gap $E_{gap}$, and the elastic modulus *B*) properties of rutile and anatase that agree better with available experimental data than the results of other calculations [22, 23]. Thus, for anatase the calculated values are: $a$ = 3.784 Å, $c$ = 9.508 Å, $u$ = 0.207, $E_{coh}$ = 18.8 eV, $E_{gap}$ = 4.1 eV, $B$ = 210 GPa, and the experimental values: $a$ = 3.782 Å, $c$ = 9.502 Å, $u$ = 0.208, $E_{coh}$ = 20.0 eV, $E_{gap}$ = 3.2 eV, $B$ = 178 GPa. Using different versions of density functional method (both in the LCAO and PW bases) the experimental data cannot be reproduced well enough. At the use of the hybrid exchange-correlation potential and the optimized atomic basis the difference between the calculated and experimental data is 0.1–0.2% in the geometrical characteristics of both crystals and no more than 5% in the characteristics of the electronic structure (except the band gap, where the

discrepancy with the experiment is higher but still remains the lowest in comparison with the data of other calculations). The choice of a calculation scheme by the quality of reproducing the experimental data by the scheme of for bulk crystals is important, because for the nanolayers and nanotubes such data are generally lacking. In addition, the below discussed estimated values for the nanolayers and nanotubes were calculated as the relative characteristics (in the first case relatively to the bulk crystal, in the second to nanolayer), which increases their reliability.

We have performed a series of calculations of the nanolayers for different anatase and rutile surfaces (see next section). For all nanolayers a stoichiometric model was considered containing an integer number of the $TiO_2$ formula units (which allows the comparison energy of nanolayer and bulk crystal). The energy of formation of the layer $E_{form}(slab)$ is estimated from the energy difference between the layer and the bulk crystal related to the $TiO_2$ formula unit:

$$E_{form}(slab) = \frac{E_n(slab)}{n} - E(bulk). \quad (3)$$

In Eq. (3) $E_n(slab)$ is the energy per a cell in the layer containing $n$ formula units, $E(bulk)$ is the energy per formula unit for the cell of the bulk crystal. In Table 2 the energies of formation are given for the nanolayers of different symmetry. Another characteristic of a nanolayer stability is the so-called surface energy $E_{surf}$ (more precisely, the potential energy of the surface formation), which is calculated by Eq. (4):

$$E_{surf}(slab) = \frac{E_n(slab) - nE(bulk)}{2S}, \quad (4)$$

where $S$ is the surface area of a biperiodical cell. As a measure of the nanotube stability relative to the layer generating it the so-called energy of strain (or energy of rolling) is commonly used:

$$E_{strain}(nt) = \frac{E_l(nt)}{l} - \frac{E_n(slab)}{n}. \quad (5)$$

In Eq. (5) $E_l(nt)$ is the energy of the relaxed nanotube containing $l$ $TiO_2$ formula units. As in the case of nanolayers, a measure of the stability of nanotube relative to the bulk phase can serve as the energy of its formation, $E_{form}(nt)$, calculated by formula (3) after replacement of $E_n(slab)$ by $E_n(nt)$. Obviously, the relation $E_{form}(nt) = E_{strain}(slab) + E_{form}(slab)$ is correct.

In the next section, we compare the results we obtained for different nanotubes based on the anatase and compare the tube formation energy for two models: with square and with hexagonal planar lattice.

## 4. Nanolayer Stability and the Models of the Nanotubes Based on Titanium Dioxide

As noted in the introduction, it is reasonable to consider the formation of nanotubes initially by examining a nanolayer cut from the bulk crystal and containing a single (as in graphite) or several (as in the case of titanium dioxide) atomic planes. The calculation of the reconstruction in a nanolayer cut from the bulk crystal allows one to offer a particular model of the nanotube obtained by rolling up the nanolayer. Finally, the calculation of various models of nanotubes allows the evaluation of the changes in the symmetry, atomic structure, and energy at the rolling nanolayer into the nanotube.

Titanium dioxide $TiO_2$ has two most stable crystalline modification: rutile and anatase. To them correspond the spatial symmetry group of the bulk crystal, $D_{4h}^{14}(P4_2/mnm)$ and $D_{4h}^{19}(P4_1/amd)$, respectively, and the tetragonal Bravais lattices, a simple (rutile) and a body centered (anatase). Both modifica-tions have two formula units of $TiO_2$ in the primitive cell. Note that the properties of thin films can differ significantly from the properties of bulk crystals. At low temperature, the bulk crystal of $TiO_2$ is more stable when it has rutile structure rather than anatase (although this difference is only 0.05 eV per formula unit, and cannot be reproduced without considering vibrational and thermal effects). As already noted, the formation of nanotubes based on $TiO_2$ does not preclude participation both rutile and anatase as the initial structures. Experiments on the synthesis of nanotubes do not show unambiguously which of the two modifications is the basis for the appearing lamellar structures [24]. There are, however, indications that, in contrast to bulk crystals, stability of nanolayers is higher for anatase compared to rutile [25]. In addition, when determining which structure of the layer is the most likely initial structure for the formation of nanotubes, not only the energy spent at cutting the layer should be considered, but also the energy of its reconstruction as compared to the bulk crystal. As will be shown below, the atomic structure of a thin layer may not correspond to any of the stable phase of titanium oxide. Also the nanotubes were synthesized with the structure of lepidocrocite (or

**Table 2.** Parameters of the optimized three- and six-plane nanolayers obtained in this work for the anatase surfaces (001) and (101)

| Model (surface) | Number of formula units in the cell | 2D cell parameters | | | Ti–O Bond length,[a] Å | $E_{form}$,[b] kJ mol$^{-1}$ | $E_{surf}$,[b] J m$^{-2}$ | $E_{gap}$,[c] eV |
|---|---|---|---|---|---|---|---|---|
| | | *a*, Å | *b*, Å | γ, ° | | | | |
| r3 (001) | 1 | 3.144 | 3.144 | 90 | 1.82 | 122.4 | 1.03 | 6.17 |
| l6 (001) | 2 | 2.979 | 3.746 | 90 | 1.82–2.17 | 29.2 | 0.44 | 5.15 |
| a3 (101) | 1 | 2.962 | 2.962 | 120 | 1.96 | 47.3 | 0.52 | 4.89 |
| a6 (101) | 4 | 3.507 | 10.335 | 90 | 1.77–2.06 | 72.6 | 0.66 | 5.97 |

[a] In the bulk crystal the calculated bond lengths are 1.93 and 1.97 Å. [b] The values are calculated relative to the anatase bulk crystal. [c] Calculated band gap in the anatase bulk crystal is 4.09 eV.

boehmite) type [26, 27], a hypothetical layered modification of titanium dioxide. The space symmetry group C*mcm* of lepidocrocite corresponds to the base-centered orthorhombic Bravais lattice containing four $TiO_2$ formula units in the primitive cell. Pairs of distorted $TiO_2$ octahedra form an infinite 6-planar layers parallel to (010) plane and separated by about 2 Å.

Experimental data on the synthesis of $TiO_2$ nanotubes indicate that the original layer in the structure of anatase is associated probably with the surface (101) as the most stable among other surfaces [25, 28, 29]. Nevertheless, of some interest is the surface of anatase (001), which, being less stable, occurs in most of anatase nanocrystals [28, 30]. However, the problem about the type of the nanolayer which would be appropriate as a source for the formation of nanotubes based on the rutile structure remains open for discussion. In [31], the nanolayer (001) is considered as such a layer since the calculation by the density functional method in PW basis of the (001) nanolayers of different thickness showed that in this case in the relaxed nanolayer sublayers arise consisting of two atomic planes (one formula unit in the square cell for each plane). Bearing in mind a disadvantage of the plane waves (PW) basis in the calculation of nanostructures with a reduced periodicity, we calculated the anatase and rutile nanolayers in the LCAO basis according to the above considered calculation scheme. As in [31], we performed a search for the nanolayers which can be used to calculate the nanotubes. It is worth to mention that the nanolayer symmetry analysis should be undertaken only after full optimization of its geometry.

A stoichiometric anatase (001) layer of minimum thickness consists of three O–Ti–O planes and to it corresponds the biperiodical group 59 ($P\bar{4}m2$). A primitive square cell contains one $TiO_2$ formula unit (model r3, Fig. 4). Titanium atoms occupy Wyckoff's nonparametric positions (located in the nodes of a square lattice), whereas the oxygen atoms occupy one-parameteric positions above and below the midpoints of adjacent sides of the square (Fig. 4). The first time geometry optimization of the tree-plane nanolayer (calculation was carried out as described above) executed by us showed that the $P\bar{4}m2$ symmetry of the biperiodical lattice is retained, but the square lattice constant is significantly reduced (from 3.78 Å to 3.14 Å), as well as the length of Ti–O bond (from 1.93 Å to 1.82 Å). Despite this, the reconstructed layer has a relatively high surface energy compared to the bulk anatase crystal (see Table 2). Note also the high value of the forbidden band gap for the electron states in the considered tetragonal layer, 6.2 eV. Thus, the monolayer exhibits the properties of a typical insulator, rather than a semiconductor.

Our calculations showed that exact the same nanolayer (Fig. 4) is obtained after reconstruction of the two-plane (001) rutile layer. As mentioned above, this layer also has a plane square lattice (biperiodical symmetry group 58, $P\bar{4}m2$) and consists of two atomic planes, that is, a $TiO_2$–$TiO_2$ bilayer, until carrying out its reconstruction. After the barrier-free reconstruction, the minimum translational cell decreases twice and space group becomes equal $P\bar{4}m2$, which leads to the identity of the reconstructed minimum (001) nanolayers of rutile and anatase. In [31], it was shown by the molecular dynamics calculations of the (001) bilayer that eventually the original square lattice is reconstructed (presumably as a result of overcoming some energy barrier) to the hexagonal, which is considered as the starting point for further calculation of nanotubes of different chirality. Note that identical hexagonal layer (Fig. 5) is obtained at the barrier-free

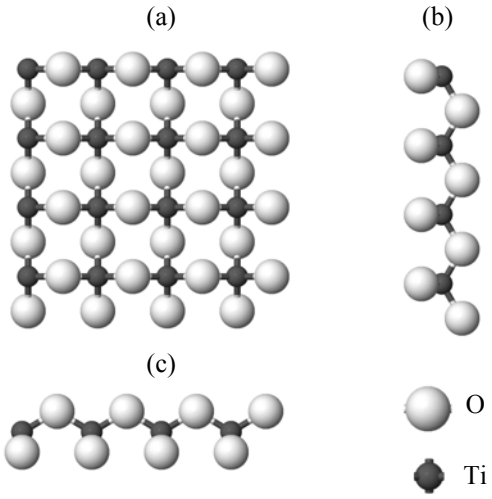


**Fig. 4.** Reconstructed anatase (001) nanolayer consisting of 3-atomic planes: (a) projection along **c** vector, (b) projection along **a** vector, (c) the projection along **b** vector.

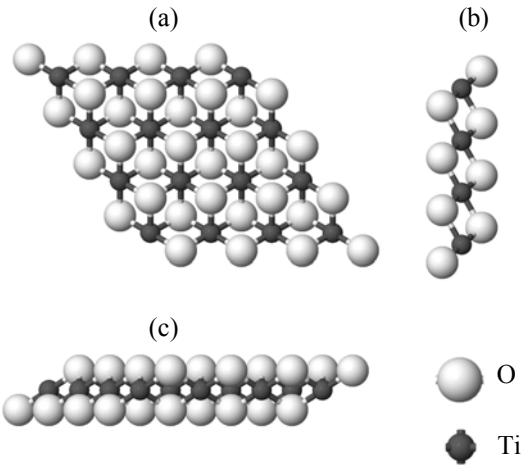


**Fig. 5.** Reconstructed anatase (101) nanolayer (101) consisting of 3-atomic planes: (a) projection along **c** vector, (b) projection along **a** vector, (c) the projection along **b** vector.

reconstruction of three-plane (101) anatase layer (see below).

As shown in several studies [30], the reconstruction of the (001) anatase layer consisting of 6 atomic planes, proceeds differently. Symmetry of the square biperiodical Bravais lattice is reduced to a primitive rectangular, and the nanolayer after reconstruction has the structure of the lepidocrocite layer (biperiodical P*mmn* group). Our calculations showed that this layer has the lowest surface energy (see Table 2) and, therefore, is the most stable compared to the anatase bulk crystal. Geometrical structure of the lepidocrocite 6-planar layer has been discussed in detail in [32].

Now let us consider the layers corresponding to the anatase (101) surface, which before the relaxation are characterized by a centered rectangular lattice and by the arrangement of atomic planes in the order of O–Ti–O. The biperiodical symmetry group of the unrelaxed layers is 18 (C2/*m*11). In the 2D unit cell of the rectangular lattice either three atomic planes (the model a3), [26, 33, 34], or six planes [12, 35] (the model a6) can be included. Like in the case of (001) surface, the relaxation of three-planar and six-planar layers proceeds differently. Calculations [31, 36] showed that in the course of the geometry optimization the planar 3-layer flat lattice is barrier-free reconstructed from rectangular into a hexagonal structure like the fluorite (111) surface (Fig. 5). The symmetry group of the reconstructed layer thus increases to P$\bar{3}$*m*1. The hexagonal primitive cell contains one $TiO_2$ formula unit (model a3). Titanium atoms occupy the nonparametric Wyckoff's positions, whereas the oxygen atoms occupy the one-parameteric positions above and below the centers of the equilateral triangles formed by the titanium atoms. The distances Ti-O in such a reconstruction practically are not affected. Our calculations show that the hexagonal monolayer has a low surface energy (see Table 2) similar in magnitude to the surface energy of the other stable $TiO_2$ monolayers [36]. This fact allows a suggestion that such layer can be obtained practically. The hexagonal nanolayer has the smallest forbidden band gap among all the layers considered in this work (see Table 2), in particular, the gap in this layer is about by 1.3 eV lower than that in the considered above tetragonal layer.

The symmetry of six-planar (101) anatase layer is not changed at the relaxation. At the same time, the atomic planes of Ti and O are shifted relative to each other so that both titanium planes almost coincide and occupy a position in the middle of the layer, while Ti–O distances vary differently along different directions. The structure of this layer was described in detail in previous papers [12, 34–36]. Calculations showed that this layer is resistant against the reconstruction and has a relatively low surface energy (see Table 2).

**Table 3.** The symmetry properties of $TiO_2$ nanotubes

| Model (surface) | Planar lattice | Biperiodical group | Chirality | Tube family | Monoperiodical group | Tube point group |
|---|---|---|---|---|---|---|
| r3 (001) | square | 59, P$\bar{4}m2$ | ($n$,0), (0,$n$) | 11 T $D_{nh}$ | **L**$n/mmm$[a] | $D_{nh}$ |
| l6 (001) | Rectangular primitive | 46, P$mmn$ | ($n$,0), (0,$n$) | 11 T $D_{nh}$ | **L**$n/mmm$[a] | $D_{nh}$ |
| a3 (101) | hexagonal | 72, P$\bar{3}m1$ | ($n$,$n$), (–$n$,2$n$), (–2$n$,$n$) | 4 $T^1_{2n}C_{nh}$ | **L**$(2n)_n/m$ | $C_{2nh}$ |
| | | | ($n$,0), (0,$n$), (–$n$,$n$) | 8 $T^1_{2n}C_{nv}$ | **L**$(2n)_nmc$ | $C_{2nv}$ |
| a6 (101) | rectangular centered | 18, C2/$m$11 | (–$n$,$n$) | 4 $T^1_{2n}C_{nh}$ | **L**$(2n)_n/m$ | $C_{2nh}$ |
| | | | ($n$,$n$) | 8 $T^1_{2n}C_{nv}$ | **L**$(2n)_nmc$ | $C_{2nv}$ |
| Graphene[b] | hexagonal | 80, P6/$mmm$ | ($n$,$n$), (–$n$,2$n$), (–2$n$,$n$) | 13 $T^1_{2n}D_{nh}$ | **L**$(2n)_n/mcm$ | $D_{2nh}$ |
| | | | ($n$,0), (0,$n$), (–$n$,$n$) | 13 $T^1_{2n}D_{nh}$ | **L**$(2n)_n/mcm$ | $D_{2nh}$ |

[a] **L**(2$n$)2m for odd $n$. [b] The symmetry of graphene nanotubes is shown for comparison with the symmetry of nanotubes of a3 (101) model and for illustration of the differences arising in various layer groups with the same flat lattice.

The symmetry properties of the examined 3- and 6-plane nanolayers and the corresponding achiral nanotubes are shown in Table 3. To determine the symmetry of the $TiO_2$ nanotubes obtained by the rolling up atomic layers we used the above-described approach for determining symmetry group of the layer after relaxation (reconstruction) and establishing the symmetry group of nanotubes, depending on the choice of the vector chirality. The symmetry analysis is performed using the above-described computer program.

In this work, to build a nanotube, we used only the models r3 and a3 (Figs. 4 and 5), which correspond to the titanium oxide nanolayers of minimum thickness. Apparently, other stable three-plane $TiO_2$ nanolayers do not exist. Therefore, further we consider in more details the symmetry and stability (see section 5) of the nanotubes formed with the models r3 and a3.

In the model r3 the flat lattice is a square. From the orthogonality relations (1) for a square lattice ($a = b$, $\gamma = 90°$) follows that the periodicity of the tube is compatible with any choice of chirality ($n_1$, $n_2$). Therewith, the symmetry group of the nanotube belongs to the family 5 with point symmetry $D_q$, because upon rolling the square layer, the rotation only around the twofold axis perpendicular to the plane of the layer survives. In the special cases of chirality ($n$,0) or (0,$n$) the symmetry of the tube increases, the symmetry group of the tube now belongs to the family 11 with point symmetry $D_{nh}$. This is due to the fact that the layer group P$\bar{4}m2$ has two symmetry planes perpendicular to the layer plane passing through the square sides, that is, through the translation vectors (1,0) and (0,1) of the square lattice, see Fig. 4. Both ($n$,0) and (0,$n$) types of rolling in the case of square lattice are equivalent, however, because the layer group 59 has no symmetry operations that ensure the equivalence of the boundary surfaces of the rolled layer, two types of tubes with the same symmetry are possible: r3' and r3".

The nanotube symmetry for the model a3 (101) is determined by the layer group 72 (P$\bar{3}m1$) with a hexagonal planar lattice (Fig. 5). As noted, for the hexagonal lattice the tube periodicity is compatible with any chirality ($n_1$, $n_2$). In contrast to the graphene layer group 80 $P6/mmm$, the layered group 72 has no second order axis perpendicular to the layer plane. Therefore, for any chirality ($n_1$, $n_2$) the nanotube in the model a3 (101) belongs to the family 1 and has the point symmetry $C_q$. Of the six planes of reflection perpendicular to the graphene layer (see Fig. 1), the group 72 contains only three rotations, each transforming into other at the 120° planes. As in the case of graphene, the chirality vector can be selected along the corresponding translation vectors of the planar hexagonal lattice, and the translation vector of the tube must be orthogonal to the chirality vector. In the model a3 (101), as in the case of graphene, two types of tubes are possible. However, unlike graphene tubes, the symmetry of the tubes of both types is different (see Table 3).

For the model a6 (101) with a centered rectangular lattice ($a = b$, $\gamma \neq 60°, 90°$) the condition (1) holds only for the tubes with the chirality ($n$,$n$) and (–$n$,$n$). The two types of tubes belong to different symmetry groups (see Table 3). The first performed full ab initio calculations of 6-plane tubes on the anatase (101) surface [12] showed that the tubes with chirality (–$n$,$n$)

are more stable than the tubes with chirality (*n*,*n*). The comparison of electronic and atomic structures and stability of 3- and 6-plane tubes on basis of the anatase (101) surface was performed in [36].

For the model l6 with the layer of lepidocrocite structure (a simple rectangular lattice, $a \neq b$, $\gamma = 90°$), as indicated in Table 3, only the chiralities (*n*,0) and (0,*n*) are compatible with the tube of a finite period. As the translation vectors *a* and *b* are unequal, the tubes with chirality (*n*,0) and (0,*n*) are different, but with the same monoperiodical symmetry group. Structure and stability of the tubes on the basis of lepidocrocite was investigated in [32].

In the next section, we discuss the results of our calculations of nanotubes constructed for the anatase surfaces (001) and (101) using the tetrahedral and hexagonal three-plane nanolayers.

## 5. Structure and Stability of Thin-Walled Nanotubes Based on Anatase

As stated above, there are two types of tubes with chirality (*n*,0), which can be obtained from the reconstructed 3-plane layer with a square lattice and the different boundary surfaces. In the tubes of the first type (r3') the Ti–O–Ti planes corresponding to bridging oxygen atoms on the inner side of the tube pass through the tube axis (Fig. 6b), and in the tubes of the second type (r3") these planes are perpendicular to the axis (Fig. 6d ). On the outer sides of the tubes the opposite is true. For each of these types we have considered two values of diameter, corresponding to $n = 6$ and $n = 12$. In addition, we performed a calculation for the (15,0) tube in the model r3". Thus, were calculated on the whole 5 different tubes built by rolling up the tetrahedral layer.

The results are listed in Table 4. These data clearly indicate that the formation of a tube of r3' type is energetically disadvantageous, both in the terms of energy for the layer rolling up, and in terms of energy of the tube formation from the bulk crystal. This is due to the fact that the distance between the bridging oxygen atoms on the inner side of the tube is smaller than the distances between them in the nanolayer and, consequently, the repulsion between them increases. Although the stability of these tubes increases with increase in the diameter (that is typical for most previously studied nanotubes [37]), the formation of such nanotubes in fact is hardly probable.

Tubes of r3" type (Figs. 6b and 6d) have a considerably lower energy of formation, and surprisingly, negative energy of the rolling. Thus, the tubes of this type are even more stable than a three-plane layer with square lattice, from which they are formed. The reason for this stabilization is not fully clear, we can only point to the increasing distance between the bridging oxygen atoms on the outer side of the tube compared with those in the nanolayer. It is also unusual that the stability of these nanotubes decreases monotonically with an increase in their diameter. If we admit the possibility of a practical synthesis of tetragonal nano-$TiO_2$, we should expect their spontaneous rolling into a small diameter nanotubes.

The simulation of nanotubes based on the hexagonal titanium dioxide layers was an object of several studies [26, 33, 36–38]. These tubes may also be of two types, depending on the chirality: *zigzag* (*n*,0) and *armchair* (*n*,*n*) (Fig. 7). For the tubes of the first type we present the results of our calculations for $n = 6$ and 12, and of the second type, for $n = 3$, 6 and 9. It follows from the data of Table 4 that the tube (6,0) differs from the other by the great positive energy of formation. The energies of rolling for the other tubes with close diameter values differ only slightly. The tubes in the model a3 with chirality (3,3) and (6,6) are close by energy to the corresponding isoatomic tubes in the model r3" with chirality (6,0) and (12,0). Our calculations showed that with increasing diameter of the tube of (*n,n*) type the energy of its formation (rolling) varies non-monotonically, passing through a maximum at low values, about 10 Å.

Previous theoretical calculations [37] showed that the nanotubes based on $TiO_2$, as well as the corresponding crystals are semiconductors with a wide forbidden gap. Our calculations fully confirm these findings. Usually, the gap width of the considered tubes has an intermediate value between the corresponding values for the bulk crystal and monolayer. As shown by our calculations, for the tubes of small diameter deviations from this rule are possible in the direction of larger values of the forbidden band gap (see Table 4).

Despite the relatively small size of the considered nanotubes, the calculations require significant computational resources. Thus, to optimize the geometry of the nanotube (12,0) in model a3 consisting of 72 atoms it took about 10 h of 24 processors with tact frequency 3 GHz.

Thus, we conclude that the possibility of formation of nanotubes is worthwhile to consider after examina-

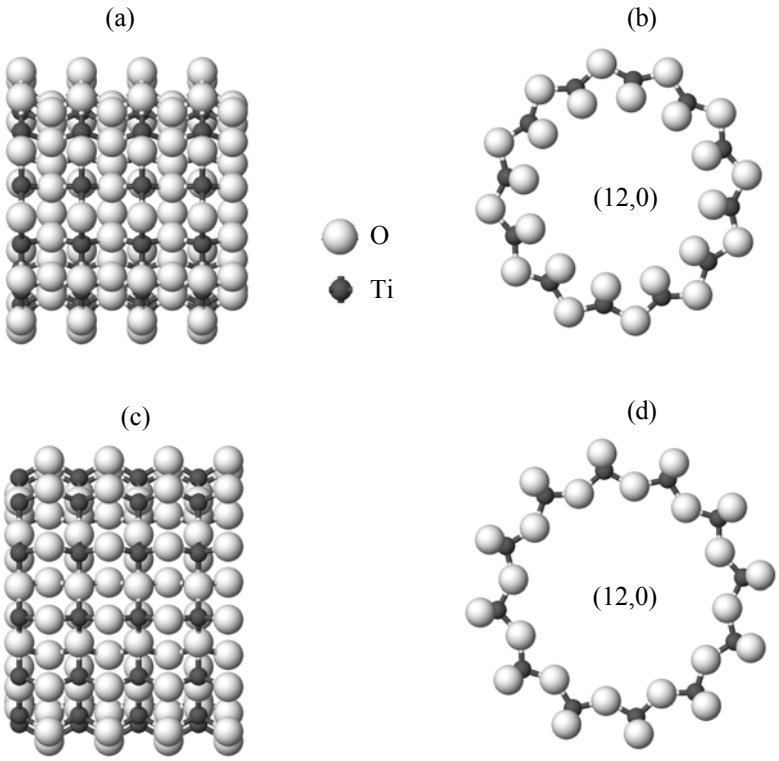


**Fig. 6.** Nanotubes obtained by the rolling up the reconstructed anatase (001) nanolayer with chiral indices (12,0) for the models (a, b) r3' and (c, d) r3"; (a, c): a projection perpendicular to the nanotube axis, (b, d): a projection parallel to the nanotube axis.

tion of the respective nanolayer cut from the bulk crystal and containing one or more atomic planes. Study of crystal surfaces that correspond to different crystallographic indices allows consideration the totality of possible nanolayers, which correspond to the stoichiometry of the crystal.

Quantum chemical calculation of relaxation or reconstruction in a nanolayer allows determination its stability and the final symmetry, and, eventually, to propose a particular symmetry model for the nanotube obtained by rolling up the respective nanolayer.

The monoperiodical symmetry group of a nanotube is unambiguosly determined by the group of reconstructed biperiodical nanolayers and the vector of rolling. To determine the specific compliance the following factors must be considered: (1) the orthogonality of the translation and rolling vectors, (2) the possibility of appearing primitive and screw symmetry axes, (3) the number and type of point symmetry operations surviving at the rolling up of the layer plane to the cylindrical surface.

The calculation of various models of nanotubes allows the evaluation of the changes in the symmetry, atomic structure, and energy at rolling a nanolayer into nanotube. Theoretical determination of the most stable types of nanotubes is essential for the creation of new nanomaterials.

On the basis of nonempirical quantum chemical calculations of the anatase monolayers consisting of 3 and 6 atomic planes we have found that the possible three-plane nanolayers have tetragonal or hexagonal structure, whereas six-plane nanolayers either retain the symmetry of the anatase (101) surface, or acquire a structure of the lepidocrocite layer distinguished by its high stability.

As a result of calculations we have shown that the titanium dioxide nanotubes of about 10 Å diameter or less, based on three-plane monolayers with hexagonal and square lattice, are approximately of the same stability. The properties of nanotubes with large diameter (>10 Å) may differ greatly from those of the tubes of small diameters.

For the first time we found that some nanotubes may have greater stability than the nanolayers from which they were created. In particular, this is observed for the nanotubes with chirality ($n$,0),

**Table 4.** Parameters of optimized nanotubes obtained at the rolling three-plane (001) and (101) anatase layers

| Tube chirality | Number of atoms in cell | Period of tube, Å | Tube diameter,[a] Å | $E_{form}$, kJ mol$^{-1}$ | $E_{strain}$, kJ mol$^{-1}$ | $E_{gap}$, eV |
|---|---|---|---|---|---|---|
| Model r3', surface (001) | | | | | | |
| (6.0) | 18 | 3.33 | 6.51 | 334.4 | 212.0 | 4.47 |
| (12.0) | 36 | 3.15 | 11.77 | 201.8 | 79.4 | 4.09 |
| Model r3", surface (001) | | | | | | |
| (6.0) | 18 | 3.16 | 7.14 | 90.7 | –31.7 | 5.47 |
| (12.0) | 36 | 3.16 | 13.10 | 97.3 | –25.1 | 5.70 |
| (15.0) | 45 | 3.16 | 16.07 | 100.1 | –22.3 | 5.77 |
| Model a3, surface (101) | | | | | | |
| (6.0) | 36 | 5.15 | 6.73 | 177.6 | 130.3 | 5.13 |
| (12.0)[b] | 72 | 5.09 | 11.70 | 80.7 | 33.4 | 4.70 |
| (3.3) | 18 | 2.87 | 6.51 | 86.5 | 39.3 | 5.47 |
| (6.6)[b] | 36 | 2.99 | 10.07 | 93.8 | 46.5 | 4.66 |
| (9.9)[b] | 54 | 2.98 | 14.88 | 67.4 | 20.1 | 4.74 |

[a] The distance from the tube axis to the titanium atoms. [b] Data of [36].

obtained by rolling up three-plane tetragonal anatase (001) layer.

The calculations presented in this paper were performed on a supercomputer complex SKIF MSU "Chebyshev."

## REFERENCES


1. Zakharova, G.S., Volkov, V.L., Ivanovskaya, V.V., and Ivanovskii, A.L., *Nanotrubki i rodstvennye nano-struktury oksidov metallov* (Nanotubes and Related Nanostructures of Metal Oxides), Yekaterinburg: Inst. Solid State Chem., 2005.
2. D'yachkov, P.N., *Uglerodnye nanotrubki. Stroenie, svoistva, primeneniya* (Carbon Nanotubes: Structure, Properties, and Application), Moscow: Binom, 2006.
3. *International Tables for Crystallography*, *Subperiodic Groups*, Kopsky, V. and Litvin, D.B., Eds., Kluwer Academic Publishers, 2002, vol. E.
4. Damnjanović, M., Nicolić, B., and Milošević, B., *Phys. Rev., B*, 2007, vol. 75, p. 033403.
5. Damnjanović, M. and Milošević, I., *Line Groups in Physics: Theory and Applications to Nanotubes and Polymers. Lecture Notes in Physics*, Berlin, Heidelberg: Springer Verlag, 2010, vol. 801, p. 180.
6. Damnjanović, M., Milošević, I., Vucović, T., and Sredanović, R., *Phys. Rev., B*, 1999, vol. 60, p. 2728.
7. *Python programming language. Python Software Foundation*, 2009, *http://www.python.org.*
8. Bahn, S.R. and Jacobsen, K.W., *Comput. Sci. Eng.,* 2002, vol. 4, p. 56.
9. Togo, A., Oba, F., and Tanaka, I., *Phys. Rev., B,* 2008, vol. 78, p. 134106-1-9.
10. Stokes, H.T., Hatch, D.M., and Campbell, B.J., *ISOTROPY User's Manual*, Provo, UT, USA, 2007; *http://stokes.byu.edu/isotropy.html*
11. Dovesi, R., Saunders, V.R., Roetti, C., Orlando, R., Zicovich-Wilson, C.M., Pascale, F., Civalleri, B., Doll, K., Harrison, N.M., Bush, I.J., D'Arco Ph., and Llunell, M., *CRYSTAL06(09) User Manual*, Turin: Univ. of Turin, 2010, *http://www.crystal.unito.it*.
12. Bandura, A.V. and Evarestov, R.A., *Surf. Sci*., 2009, vol. 603, p. L117.
13. Damnjanović, M., Milošević, I., Vucović, T., Dobardzić, E., and Nikollić, B., *Phys. Rev., B*, 2004, vol. 69, p. 153401
14. Ernzerhof, M. and Scuseria, G.E., *J. Chem. Phys*., 1999, vol. 110, p. 5029.
15. D'yachkov, P.N., and Makaev, D.V., *Phys. Rev., B*, 2007, vol. 76, p. 195411.
16. Evarestov, R.A., *Quantum Chemistry of Solids. The LCAO First Principles Treatment of Crystals. Springer Series in Solid State Sciences*, Berlin: Springer Verlag, 2007, vol. 153, p. 558.
17. Hurley, M.M., Pacios, L.F., Christiansen, P.A., Ross, R.B., and Ermler, W.C., *J. Chem. Phys*., 1986, vol. 84, p. 6840.

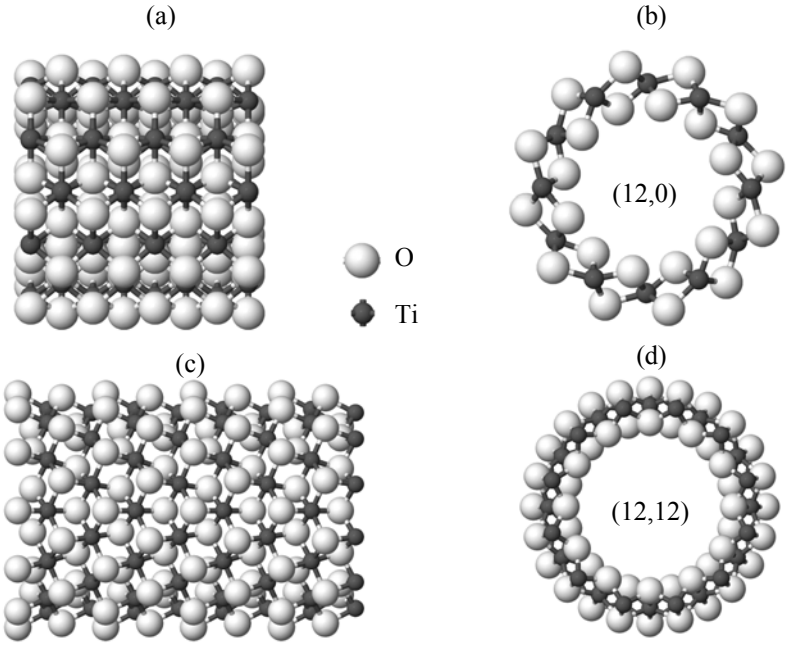


**Fig. 7.** Nanotubes obtained by the rolling up the reconstructed anatase (101) nanolayer with chiral indices (a, b) (12,0) and (c, d) (12,12) for model a3. Views (a, c): a projection perpendicular to the nanotube axis, views (b, d): a projection parallel to the nanotube axis.


18. Schäfer, A., Huber, C., and Ahlrichs, R., *J. Chem. Phys*., 1994, vol. 100, p. 5829.
19. Press, W.H., Teukolsky, S.A., Vetterling, W.T., and Flannery, B.P., *Numerical Recipes in Fortran 77*, 2nd ed., Cambidge Univ. Press, Cambridge, MA, 1997.
20. Evarestov, R.A., Panin, A.I., Bandura, A.V., and Losev, M.V., *J. Phys. Conf. Ser*., 2008, vol. 117, p. 012015.
21. Monkhorst, H.J. and Pack, J.D., *Phys Rev., B*, 1976, vol. 13, p. 5188
22. Peng, H., *Phys. Lett., A*, 2008, vol. 372, p. 1527.
23. Labat, F., Baranek, P., Domain, C., Minot, C., and Adamo, C., *J. Chem. Phys*., 2007, vol. 126, p. 154703.
24. Maiyalagan, T., Viswanathan, B., and Varadaraju, U.V., *Bull. Mater. Sci*., 2006, vol. 29, p. 705.
25. Labat, F., Baranek, P., and Adamo, C., *J. Chem. Theory Comput*., 2008, vol. 4, p. 341.
26. Enyashin, A.N. and Seifert, G., *Phys. Stat. Sol., B,* 2005, vol. 242, p. 1361.
27. Ma, R., Bando, Y. and Sasaki, T., *Chem. Phys. Lett.,* 2003, vol. 380, p. 577.
28. Vittadini, A., Casarin, M., and Selloni, A., *Theor. Chem. Acc*., 2007, vol. 117, p. 663.
29. Lazzeri, M., Vittadini, A., and Selloni, A., *Phys. Rev., B*, 2001, vol. 63, p. 155409.
30. Vittadini, A. and Casarin, M., Theor. Chem. Acc., 2008, vol. 120, p. 551.
31. He, T., Zhao, M., Zhang, X., Zhang, H., Wang, Z., Xi, Z., Liu, X., Yan, S. Xia, Y., and Mei, L., J. *Phys. Chem., C*, 2009, vol. 113, p. 13610.
32. Szieberth, D., Ferrari, A.M., Noel, Y., and Ferrabone, M., *Nanoscale*, 2010, vol. 2, p. 81.
33. Wang, J., Wang, L., Ma, L., Zhao, J., Wang, B., and Wang, G., *Physica, E*, 2009, vol. 41, p. 838
34. Liu, Z., Zhang, Q., Qin, L.C., *Solid State Comm*., 2007, vol. 141, p. 168.
35. Lin, F., Zhou, G., Li, Z., Li, J., Wu, J., and Duan, W., *Chem. Phys. Lett*., 2009, vol. 475, p. 82
36. Evarestov, R.A., Bandura, A.V. Losev, M.V., Piskunov, S., and Zhukovskii, Yu.F., *Physica, E*, 2010 (in press).
37. Enyashin, A.N., Gemming, S., and Seifert, G., *Simulation of Inorganic Nanotubes, Materials for Tomorrow. Theory, Experiments and Modelling,* Springer Series in Materials Science, 2007, vol. 93, 2007, p. 33.
38. Ivanovskaya, V.V., Enyashin, A.N., and Ivanovskii, A.L., *Mendeleev Commun*., 2003, vol. 13, p. 5.